Electronic supporting information

Steric Hindrance-Induced Selective Growth of Rhodium on Gold Nanobipyramids for Plasmon-Enhanced Nitrogen Fixation

Henglei Jia,[a,‡] Fan Li,[a,‡] Yuanyuan Yang[a], Mengxuan Zhao[a], Jingzhao Li[a] and Chun-yang Zhang*[a,b]

[a] College of Chemistry, Chemical Engineering and Materials Science, Shandong Normal University, Jinan 250014, China

[b] School of Chemistry and Chemical Engineering, Southeast University, Nanjing 211189, China.

* Corresponding author. E-mail: cyzhang@sdnu.edu.cn

‡ These authors contributed equally to this work.

Supporting Experimental Section

Chemicals. Sodium borohydride ($NaBH_4$, 99%), hexadecyltrimethylammonium bromide (CTAB, for molecular biology, ≥ 99.0%), benzyldimethylhexadecylammonium chloride (16-BAC, cationic detergent), sliver nitrate ($AgNO_3$, ≥ 99.0%), L-ascorbic acid (AA, ≥ 99.0%), sodium citrate tribasic dihydrate (TSC, ≥ 99.0%), sodium hydroxide (NaOH, ≥ 97.0%, pellets), sodium iodide (NaI, ≥ 99.5%) and methanol (CH_3OH, for HPLC, ≥ 99.9%) were purchased from Sigma-Aldrich. Tetrachloroauric (Ⅲ) acid tetrahydrate ($HAuCl_4 \cdot 4H_2O$), hydrochloric acid (HCl, ~36.0–38.0 wt%), ammonia solution ($NH_3 \cdot H_2O$, ~25.0–28.0 wt%), and hydrogen peroxide (H_2O_2, ≥ 30.0 wt%) were obtained from Sinopharm Chemical Reagent. Rhodium (Ⅲ) chloride trihydrate ($RhCl_3 \cdot 3H_2O$, 98.0%), hexadecyltrimethylammonium chloride (CTAC, 97%), ammonium chloride (NH_4Cl, PT), salicylic acid ($C_6H_4(OH)COOH$, ≥ 99.0%), and sodium hypochlorite solution (NaClO, available chlorine ≥ 5.0%) were purchased from Aladdin Reagent. Sodium nitroferricyanide (Ⅲ) dihydrate ($Na_2[Fe(CN)_5NO] \cdot 2H_2O$, 99%) was obtained from Macklin. Nitrogen ($^{14}N_2$, 99.999%), nitrogen ($^{15}N_2$, 98 atom% ^{15}N) and argon (Ar, 99.999%) was used as received. Deionized (DI) water with a resistivity of 18.2 MΩ·cm was used in all procedures.

Growth of the Au NBPs. The Au NBP sample for Rh overgrowth was prepared using a seed-mediated growth method, as described in previous works.[1] Specifically, the seed solution was made by adding a freshly prepared, ice-cold $NaBH_4$ solution (0.01 M, 125 μL) into a mixture solution of $HAuCl_4$ (0.01 M, 125 μL), TSC (0.01 M, 250 μL), and DI water (9.625 mL) under vigorous stirring. The resultant seed solution was kept undisturbed in an oven set at 30 °C for at least 2 h. The seed solution (200 μL) was then added into a growth solution that was prepared by mixing CTAB (0.1 M, 40 mL), $HAuCl_4$ (0.01 M, 2 mL), $AgNO_3$ (0.01 M, 400 μL), HCl (1 M, 800 μL), and AA (0.1 M, 320 μL) in advance, followed by gentle inversion mixing for 10 s. The resultant solution was kept undisturbed in an oven set at 30 °C overnight. The as-obtain Au NBPs were further purified through a depletion-force-induced purification process.

Growth of the Au NBP/tip-Rh NDs. The as-grown Au NBPs (optical density (OD) at the major plasmon peak pre-adjusted to 3.0, 5 mL) were centrifugated once and redispersed into DI water (500 μL) for further use. For the selective growth of Rh nanocrystals on two tips of Au NBPs, 16-BAC (0.01 M, 70 μL), $RhCl_3$ (0.01 M, 200 μL), Au NBPs (500 μL), NaI (1 mM, 20 μL) and AA (0.1 M, 200 μL) were sequentially added into DI water (9.01 mL) in a scintillation vial (20 mL) under magnetic stirring. The overall volume of the mixture solution was 10 mL and the final concentration of 16-BAC was 70 μM. The resultant solution was placed in an oven set at 95 °C for 1 h. The color of the solution was changed from red to gray after the growth process.

Growth of the Au NBP@Rh core@shell nanostructures. The preparation of Au NBP@Rh core@shell nanostructures was similar to that of dumbbell-shaped nanostructures except that the final concentration of 16-BAC was adjusted to 10 μM and the amount of NaI was increased to 100 μL. The overall volume was adjusted to 10 mL using DI water.

Growth of the Rh nanocrystals. The preparation of Rh nanocrystals was similar to that of dumbbell-shaped nanostructures except that Au NBP sample (0.5 mL) was replace with DI water (0.5 mL).

Photocatalytic N_2 fixation. The N_2 photofixation experiments were conducted in a home-made photocatalytic reactor with three ends, of which two side ends were used for gas inlet and outlet and one middle end (diameter = 3 cm) was equipped with a quartz window for light illumination. Take dumbbell-shaped nanostructures as an example, the catalyst (0.26 mg) was washed with water to remove excess surfactant and was redispersed into DI water (8 mL). To close the photocatalytic cycle, CH_3OH (2 mL) was used as the hole scavenger. Pior to each experiment, high-purity N_2 (20 mL min^{-1}) was pumped into the reaction solution at a pressure of 1 atm for 30 min under gentle stirring. A continuous Xe lamp (CEL-HXF300) was employed as the light source for the illumination and two filters (CEL-AM1.5G and CEL-JB420) were equipped on the Xe lamp to supply a visible–near-infrared (NIR) light ($\lambda > 420$ nm, 400 mW cm^{-2}). The reaction solution temperature was kept at 25 °C using a water-circulation cooling system. The N_2 photofixation experiment was conducted for 2 h and a

small amount of reaction solution (0.75 mL) was taken out for each 30 min. The production of NH_3 was quantitatively detected with the indophenol-blue method.[2,3]

Density functional theory calculation. The DFT calculations were carried out using the projector augmented plane-wave method, as implemented in the Vienna *ab initio* simulation package (VASP).[4] The exchange-correlation potential was described by the generalized gradient approximation (GGA) with the Perdew–Burke–Ernzerhof (PBE) formulation.[5] The cut-off energy of plane wave and the convergence criterion in iterative solution of the Kohn-Sham equation were set to 450 eV and 10^{-5} eV, respectively. The Brillouin zone was sampled with 2 ×2 × 1 k-mash, and a vacuum layer of 20 Å was added along z direction. During geometry optimization, all atoms of the structure were relaxed. The change of Gibbs free energy (ΔG) on the Au/Rh catalyst surface was calculated according to equation 1.

$$\Delta G = \Delta E + \Delta E_{\mathrm{ZPE}} - T\Delta S \qquad (1)$$

where ΔE, ΔE_{ZPE}, and ΔS are the changes of electronic energy, zero-point energy, and entropy, respectively. T is set as the room temperature (T = 298.15 K).

Characterization. Transmission electron microscopy (TEM) imaging was performed on an HT7700 electron microscope operated at 100 kV. The aberration-corrected high-resolution TEM (HRTEM) imaging, high-angle annular dark-field scanning transmission electron microscopy (HAADF-STEM) imaging, and energy-dispersive X-ray (EDX) elemental mapping were conducted on an FEI Titan Themis G2 microscope operated at 300 kV. The extinction spectra were measured on a Hitachi U-3900 ultraviolet/visible/NIR spectrophotometer. X-ray diffraction (XRD) patterns were acquired on a Smart Lab Se diffractometer equipped with Cu Kα radiation. X-ray photoelectron spectroscopy (XPS) spectra were measured on a Thermo Scientific ESCALAB 250Xi spectrometer equipped with an Al Kα X-ray source (hν = 1486.6 eV). Inductively coupled plasma optical emission spectroscopy (ICP-OES) was conducted on a PerkinElmer Optima 7300 DV system.

Supplementary Figures

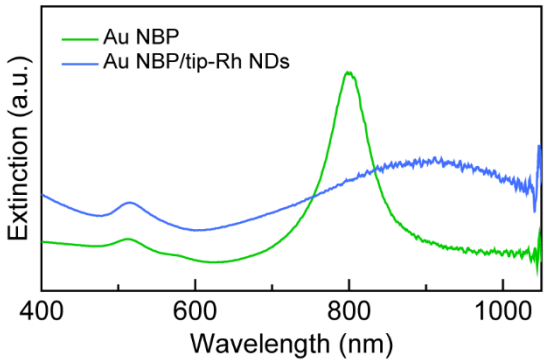

Fig. S1 Extinction spectra of the Au NBPs before (green) and after (blue) the selective growth of Rh nanocrystals.

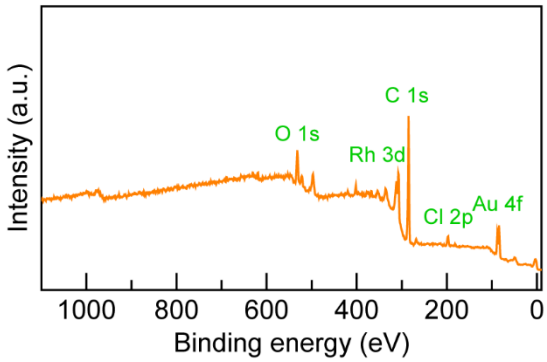

Fig. S2 XPS survey spectrum of the Au NBP/tip-Rh NDs.

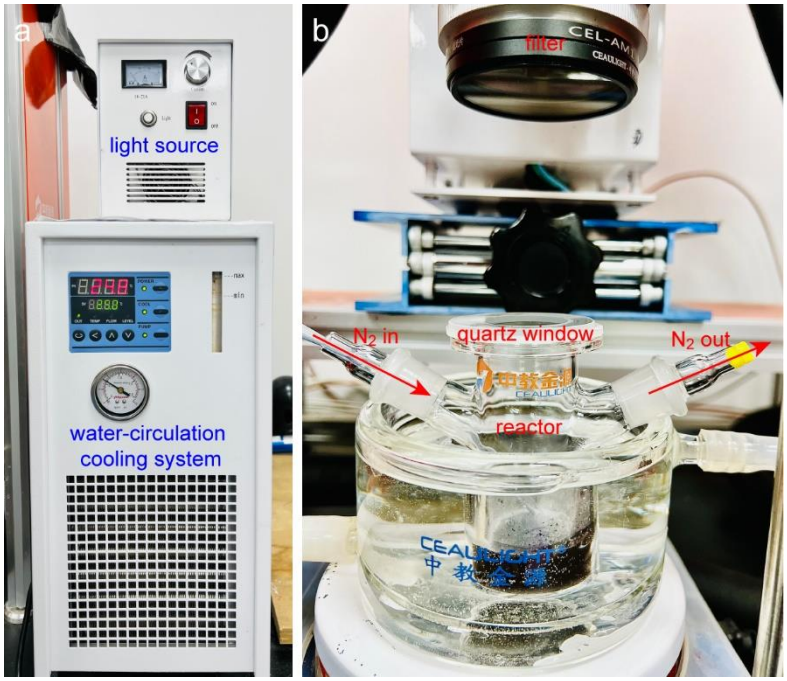

Fig. S3 Photographs of the photocatalytic system for N_2 photofixation. (a) Light source and water-circulation cooling system. (b) Photocatalytic reaction devices.

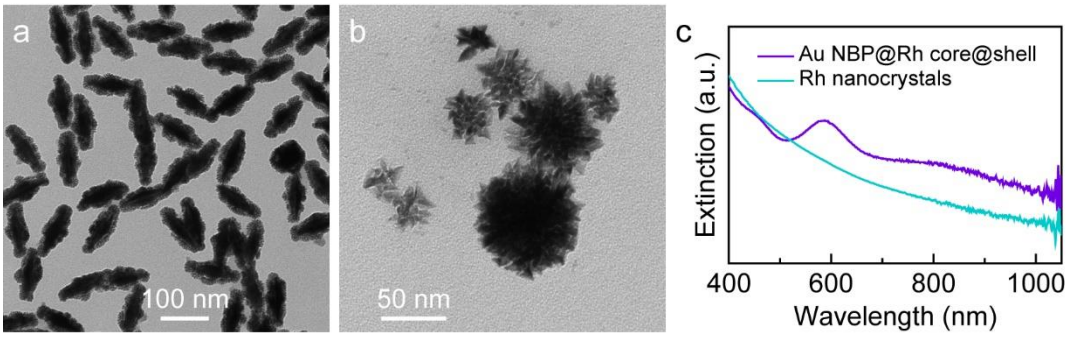

Fig. S4 (a) TEM image of the Au NBP@Rh core@shell nanostructures. (b) TEM image of the Rh nanocrystals. (c) Extinction spectra of the Au NBP@Rh core@shell nanostructures and Rh nanocrystals.

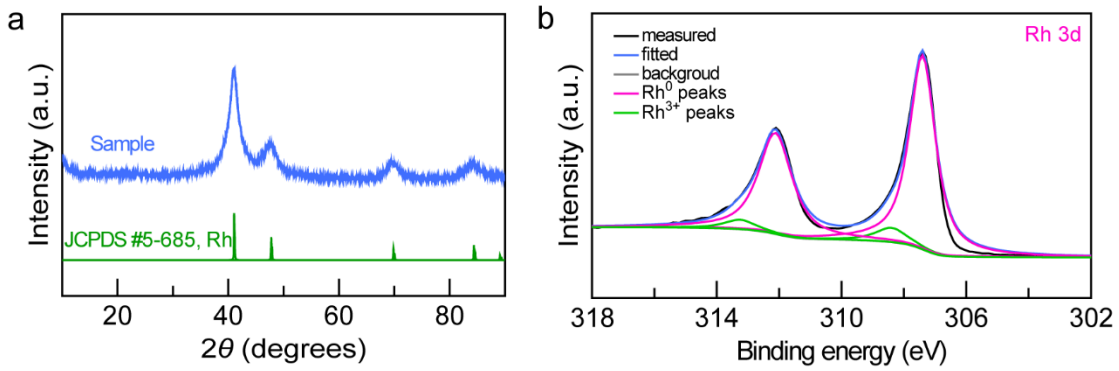

Fig. S5 (a) XRD patterns of the Rh nanocrystals. The green curve is the standard powder diffraction patterns of the face-centered-cubic structure of Rh (space group, F*m*-3*m*; lattice constant, 0.38031 nm). (b) High-resolution Rh 3d XPS spectra of the Rh nanocrystals.

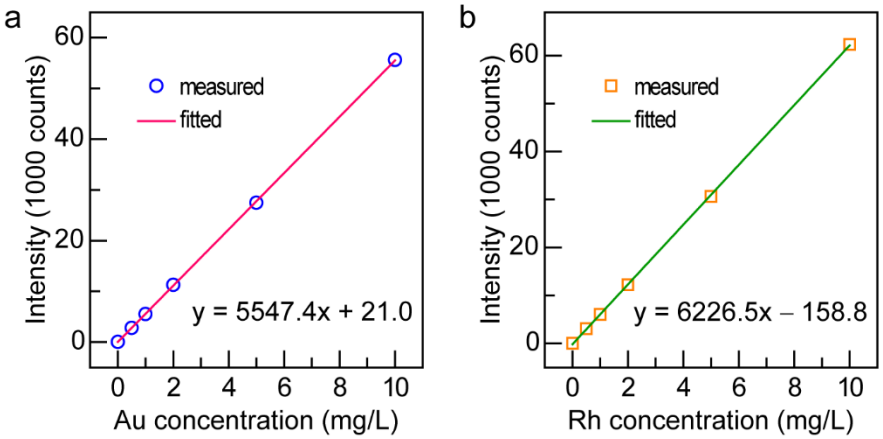

Fig. S6 Linear calibration relationships between the emission intensity and the atomic mass concentration for Au and Rh in the ICP-OES measurements. (a) For Au. The coefficient of determination for the linear fitting is R^2 = 0.99993. (b) For Rh. The coefficient of determination for the linear fitting is R^2 = 0.99991.

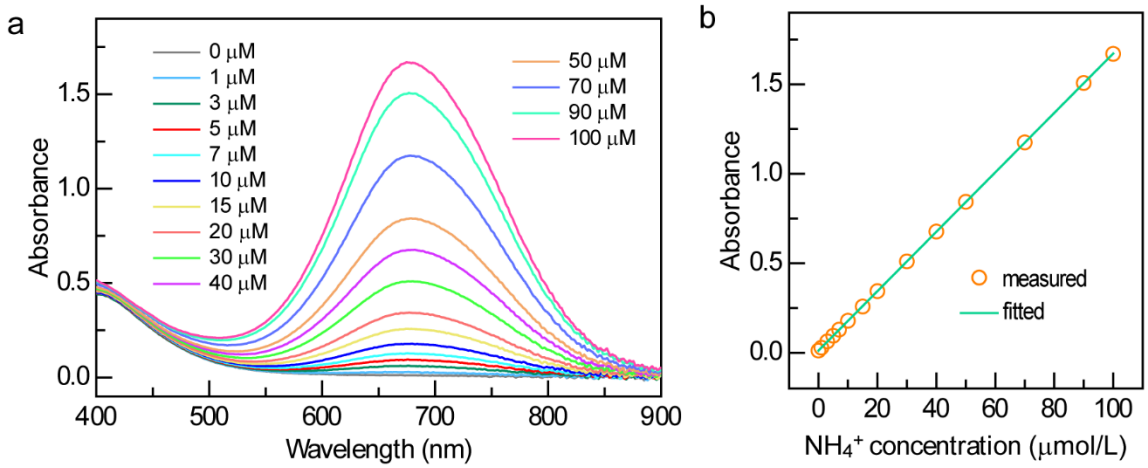

Fig. S7 (a) Absorption spectra of the standard NH_4Cl solutions with different concentrations. (b) Linear relationship between the absorbance values and concentrations of the standard NH_4Cl solutions. The coefficient of determination for the linear fitting is R^2 = 0.99999.

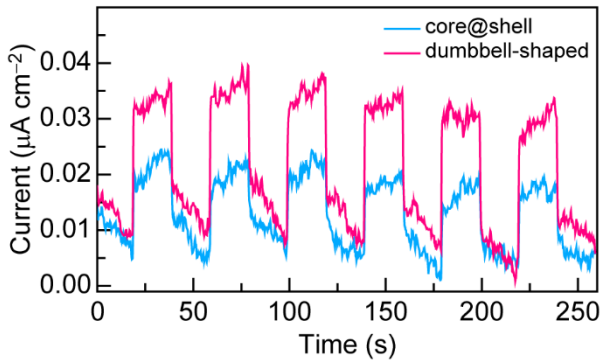

Fig. S8 Time-dependent photocurrent of the core@shell and dumbbell-shaped Au/Rh nanostructures measured at the open-circuit potential under visible–NIR light illumination.

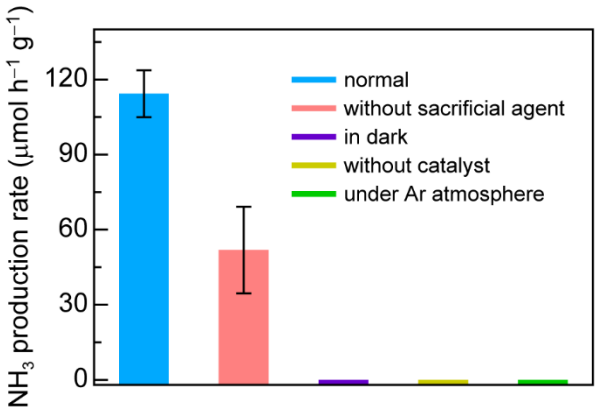

Fig. S9 Control experiments of the N_2 photofixation under different conditions.

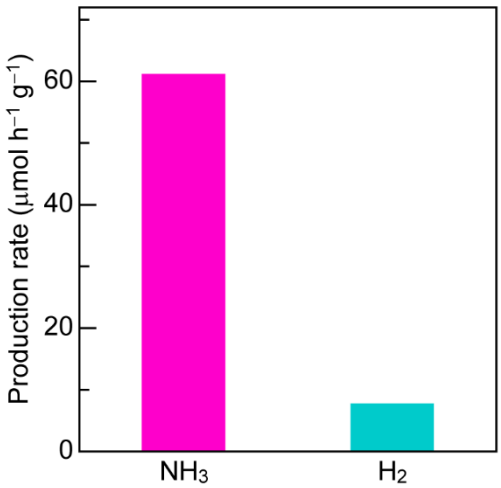

Fig. S10 Competition between NH_3 synthesis and H_2 evolution on the Au NBP/tip-Rh NDs. The photocatalytic reaction was conducted in a gastight glass reactor (65 mL). Specifically, the Au NBP/tip-Rh ND sample (0.26 mg) was added into a mixture solution of DI water (16 mL) and CH_3OH (4 mL). Prior to the illumination, the resultant solution was purged with Ar gas and then bubbled with N_2 gas (20 mL min^{-1}) for 1h. The reactor was sealed and the product generation rates were determined after 2-h light illumination ($\lambda > 420$ nm, 400 mW cm^{-2}).

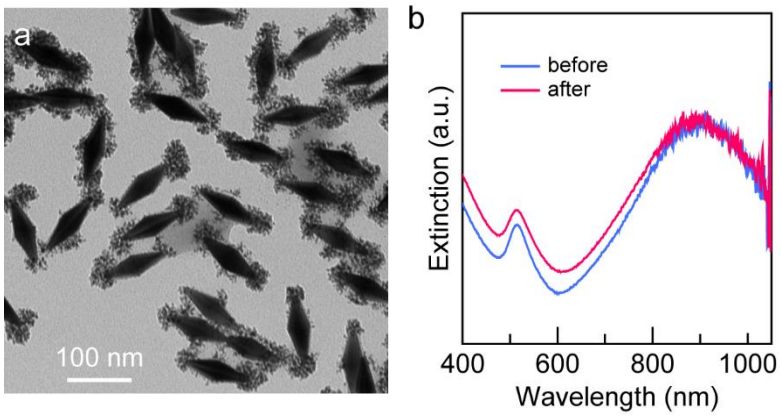

Fig. S11 (a) TEM image of the Au NBP/tip-Rh NDs after the photocatalytic reaction. (b) Extinction spectra of the Au NBP/tip-Rh NDs before (blue) and after (red) the photocatalytic reaction.

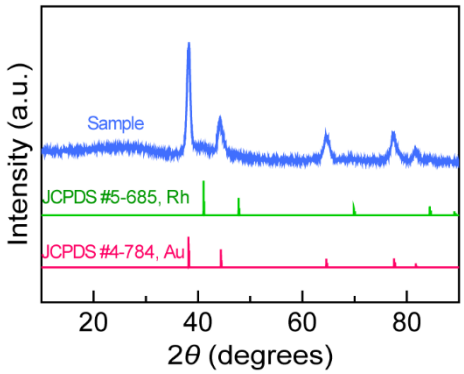

Fig. S12 XRD patterns of the Au NBP/tip-Rh NDs after the photocatalytic reaction. The red and green curves are the standard powder diffraction patterns of the face-centered-cubic structure of Au (space group, F*m*-3*m*; lattice constant, 0.40786 nm) and the face-centered-cubic structure of Rh (space group, F*m*-3*m*; lattice constant, 0.38031 nm).

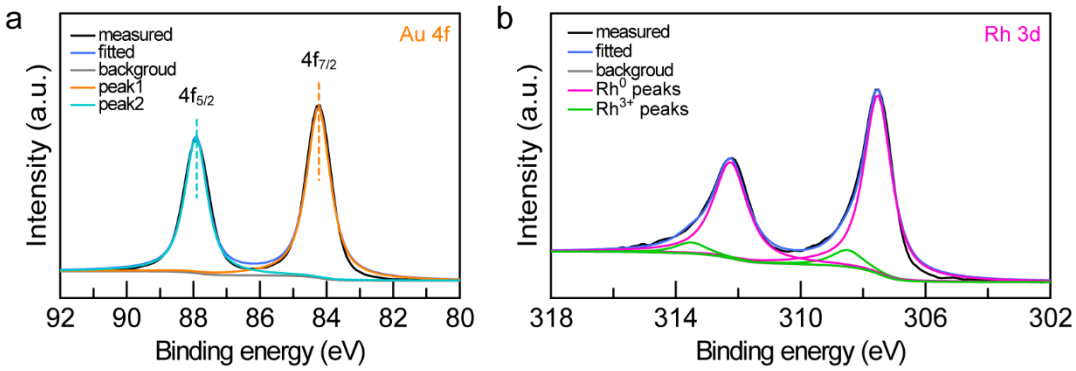

Fig. S13 (a, b) High-resolution Au 4f (a) and Rh 3d (b) XPS spectra of the Au NBP/tip-Rh NDs after the photocatalytic reaction.

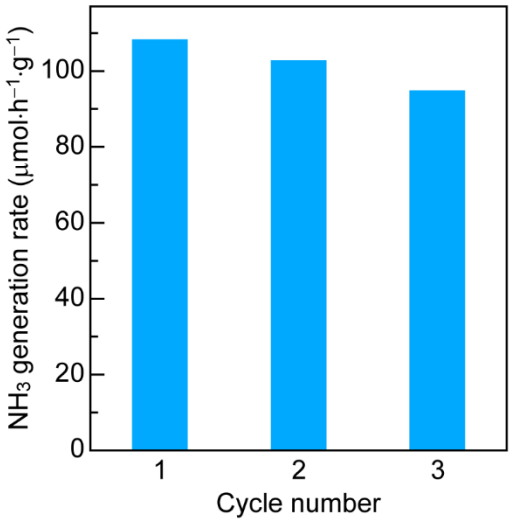

Fig. S14 N_2 photofixation activities of three successive cycles with the Au NBP/tip-Rh NDs as the catalyst.

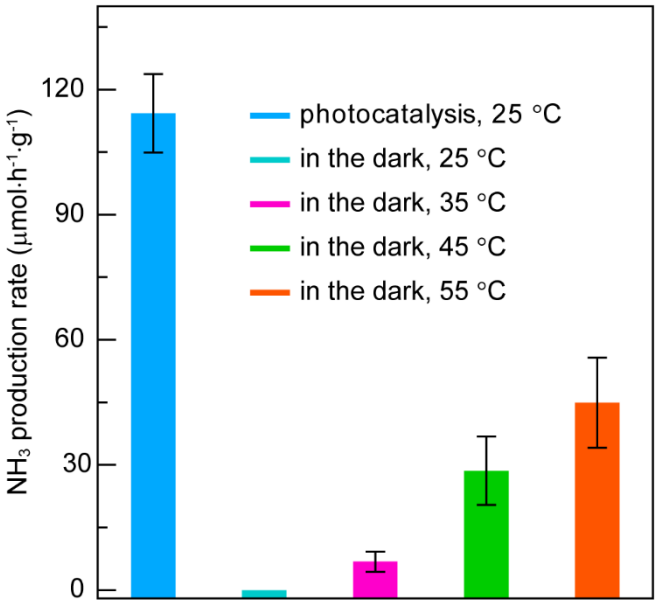

Fig. S15 Comparison of the catalytic activities performed under light illumination and in different-temperature water baths in the dark.

Supplementary Figure

Table S1. The weights of the different catalysts used for the N_2 photofixation.

catalyst	mass of Au (mg)	mass of Rh (mg)	Total mass (mg)
Au NBP/tip-Rh NDs	0.17	0.09	0.26
Au NBP@Rh core@shell nanostructures	0.20	0.17	0.37
Au NBPs	0.52	0.00	0.52
Rh nanocrystals	0.00	0.50	0.50
the mixture of Au NBPs with Rh nanocrystals	0.27	0.16	0.43

References

1. Q. Li, X. L. Zhuo, S. Li, Q. F. Ruan, Q.-H. Xu and J. F. Wang, *Adv. Opt. Mater.*, 2015, **3**, 801–812.

2. J. H. Yang, Y. Z. Guo, R. B. Jiang, F. Qin, H. Zhang, W. Z. Lu, J. F. Wang and J. C. Yu, *J. Am. Chem. Soc.*, 2018, **140**, 8497–8508.

3. H. L. Jia, A. X. Du, H. Zhang, J. H. Yang, R. B. Jiang, J. F. Wang and C.-y. Zhang, *J. Am. Chem. Soc.*, 2019, **141**, 5083–5086.

4. G. Kresse and D. Joubert, *Phys. Rev. B*, 1999, **59**, 1758–1775.

5. J. P. Perdew, K. Burke and M. Ernzerhof, *Phys. Rev. Lett.*, 1996, **77**, 3865–3868.